Projection of changes in the frequency of heavy rain events over Hawaii based on leading Pacific climate modes

O. Elison Timm,[1] H. F. Diaz,[2] T. W. Giambelluca,[3] and M. Takahashi[3]

Received 18 August 2010; revised 21 November 2010; accepted 28 December 2010; published 23 February 2011.

[1] This study investigates the frequency of heavy rainfall events in Hawaii during the wet season (October-April) 1958–2005 and their conditional dependence on the Pacific-North American (PNA) pattern and El Niño-Southern Oscillation (ENSO). Heavy rain events are defined by the 95% quantile in the rainfall distribution of the wet seasons. Twelve stations with daily reports of rainfall amounts were used to count the number of heavy rain days during wet seasons. Multiple linear regression (MLR) indicated that the PNA index (PNAI) and the Southern Oscillation Index (SOI) can explain a significant amount of the interannual to interdecadal variability for 9 out of 12 stations. Cross validation showed that PNAI and SOI together explain about 18–44% of the variability in the number of heavy rain events. Furthermore, the MLR model reproduces the trend toward fewer heavy rain events in the years after the Pacific climate shift in the mid-1970s. The MLR model was applied to the projected PNAI and SOI indices that were obtained from six IPCC AR4 climate models. The current suite of AR4 simulations based on the A1B and A2 emissions scenarios projects small and equivocal changes in the mean state of the SOI and PNAI during the 21st century. The covariance between PNAI and SOI in these simulations appears to be stable. To the extent that variations in the frequency and magnitude of ENSO and the PNA mode are responsible for modulating extreme rainfall occurrence in Hawaii, our results indicate small changes in the projected number of heavy rainfall days with large uncertainties resulting from disparities among the climate models.

Citation: Elison Timm, O., H. F. Diaz, T. W. Giambelluca, and M. Takahashi (2011), Projection of changes in the frequency of heavy rain events over Hawaii based on leading Pacific climate modes, *J. Geophys. Res.*, *116*, D04109, doi:10.1029/2010JD014923.

1. Introduction

[2] Current trends in temperature and rainfall have been identified as major stress factors for many endemic species in Hawaii's unique ecosystem. Facing the potential threat of future climate change, conservation management and water resource management will require new adaptive approaches. Previous studies have screened the 20th century climate for trends in temperature and precipitation. A general warming trend that increases with altitude was detected [*Giambelluca et al.*, 2008]. Rainfall data and stream discharge data show a trend toward lower annual mean precipitation [*Diaz et al.*, 2005; *Oki*, 2004], and a reduction in the number and intensity of extreme rainfall events [*Chu et al.*, 2009; *Chu et al.*, 2010]. The regional changes in climate variables such as temperature and precipitation have been observed on decadal and multidecadal time scales, but a formal attribution to either natural intrinsic variability of the ocean-atmosphere system, natural external climate forcing, or man-made greenhouse gas forcing cannot be achieved with the available observational data. It is one of the major efforts behind the formal detection and attribution of regional climate change which attempts to combine local observations with climate modeling studies to optimize the fingerprint of anthropogenic climate change [*Zwiers and Zhang*, 2003; *Hegerl et al.*, 2004; *Zhang et al.*, 2007; *Stott et al.*, 2010]. Without understanding the ultimate cause of trend-like features, extrapolation into the mid and late 21st century must be considered with caution.

[3] Very few studies have been devoted to future projections of regional climate change for Hawaii. Two approaches can be applied to refine the coarse-resolution global climate change scenarios: dynamical and statistical downscaling. Whereas the former makes use of a computationally expensive regional climate model, the latter approach deploys various types of statistical methods to quantify some characteristics of the underlying joint probability distribution between regional climate variables and the large-scale climate variability [*Christensen et al.*, 2007].

[1] International Pacific Research Center, SOEST, University of Hawai'i at Mānoa, Honolulu, Hawaii, USA.
[2] Climate Diagnostics Center, NOAA-CIRES, Boulder, Colorado, USA.
[3] Department of Geography, University of Hawai'i at Mānoa, Honolulu, Hawaii, USA.

0148-0227/11/2010JD014923

Table 1. Rain Gauge Stations Used in the Analysis[a]

Number	Station Identification	Name	Lon. (°E)	Lat. (°N)	Elev. (m)	Missing Obs. (%) 1958–1976 (1977–2005)	Prob. Rain (%) 1958–1976 (1977–2005)	p_{95} (mm) 1958–1976
1	511004	HALEAKALA R S 338	−156.224	20.758	2121	0.7 (1.0)	42.9 (39.4)	50.8
2	511303	HAWAII VOLCNS NP HQ 54	−155.244	19.426	1210	1.5 (4.8)	79.5 (77.4)	47.5
3	511492	HILO INTERNATIONAL AP	−155.047	19.720	12	0.0 (0.5)	71.5 (68.7)	55.4
4	511919	HONOLULU INTL AP 703	−157.911	21.320	2	0.8 (0.0)	31.8 (27.8)	36.3
5	512572	KAHULUI WSO AP 398	−156.410	20.893	16	0.0 (0.1)	32.6 (31.7)	27.2
6	512679	KAILUA 446	−156.191	20.889	213	7.7 (31.4)	74.6 (68.7)	51.8
7	512751	KAINALIU 73.2	−155.909	19.535	457	4.9 (28.1)	43.8 (30.1)	35.1
8	512286	LANAI CITY 672	−156.915	20.824	494	12.3 (32.2)	37.9 (26.6)	37.8
9	515580	LIHUE WSO AP 1020.1	−159.329	21.984	30	0.0 (0.0)	54.5 (52.6)	33.3
10	516198	MAUNA LOA SLOPE OBS	−155.559	19.537	3399	1.4 (15.0)	22.8 (10.8)	24.4
11	516588	NAALEHU 14	−155.578	19.067	244	24.4 (9.5)	40.7 (34.5)	46.2
12	517166	OPIHIHALE 2 24.1	−155.860	19.271	415	1.7 (<0.1)	46.3 (35.6)	26.7

[a]Data were extracted from the "summary of the day" data set available from the National Climatic Data Center, NOAA, in Asheville, North Carolina. Missing observations and the chance of rain are presented for the two subperiods 1958–1976 and 1977–2005. The probability of rain is defined as the ratio between the number of days with measurable rainfall (>0.254 mm/d) and the number of rain and dry days. Column p_{95} shows the 95% quantile of the cumulative rainfall distribution obtained from all rain days during 1958–1976 wet seasons (October-April). Lon., longitude; Lat., latitude; Elev., elevation; Missing Obs., missing observation; Prob. Rain, probability of rain.

Although the statistical problem may be considered well-defined in the framework of statistical theories, the practical limitations for applying statistical downscaling techniques vary from case to case [*Wilby and Wigley*, 1997]. In Hawaii, for example, it is the interaction between the topography and the general circulation that produces a spatially heterogeneous climate pattern. Steep topographic gradients are responsible for the complex pattern in rainfall and vegetation zones which are characterized by very short horizontal and vertical scales. Despite the rather dense network of rain gauges in the major islands of Hawaii, it is clear that only a fraction of the full spatial covariance structure in the rainfall is represented in the observational records, which imposes a major challenge not only to statistical downscaling methods but also to any regional climate model verification. *Timm and Diaz* [2009] were the first to attempt a synoptic-statistical downscaling procedure to estimate future changes in the seasonal mean rainfall at individual stations. They found that the ensemble mean scenario for the AR4 scenario A1B simulations suggests slightly reduced rainfall (5%) during the wet season and a weak increase during the dry season (5–10%) on average over Hawaii. In many environmental impact studies, changes in the mean are of less concern than extreme events. Heavy rainfall can cause severe flash floods, erosion and riverine influx of debris with severe effects on coral ecosystems, riparian zones, and increased threat to life and property.

[4] An essential component of statistical downscaling is the diagnostic analysis of the past, instrumentally observed climate variability. Hawaii is located in the latitude belt of the descending branch of the Hadley circulation with prevailing northeasterly trade winds in the lower atmosphere, frequently accompanied by a pronounced trade wind inversion layer [*Cao et al.*, 2007]. However, during the wet season months October– April, extratropical cyclonic disturbances and their frontal systems contribute significantly to the annual rainfall in Hawaii [*Lyons*, 1982; *Schroeder*, 1993]. Strong influences from tropical ENSO climate variability and extratropical variability associated with the Pacific Decadal Oscillation (PDO) [*Mantua and Hare*, 2002] have been observed in the past decades [*Chu*, 1989; *Chu and Chen*, 2005].

[5] Despite a multitude of studies that have investigated future changes in ENSO variability and mean shifts in the tropical climate [*Collins*, 2005; *Latif and Keenlyside*, 2009; *Vecchi and Wittenberg*, 2010; *Collins et al.*, 2010], current projections of warming-induced changes are still uncertain. A large spread exists among the IPCC AR4 models, however, the latest studies indicate that more models tend toward a climate mean state that resembles an El Niño-like pattern [*Vecchi and Wittenberg*, 2010]. The tendency in terms of ENSO variance is also uncertain, and current projections from the AR4 models range from reduced to increased ENSO variability. Furthermore, it is unclear how the covariance between tropical and extratropical climate modes such as ENSO and PNA will be affected in future climate change scenarios.

[6] In this study, we estimate (1) how the frequency of heavy rainfall events has varied in the last 50 years and (2) how these changes are correlated with the large-scale climate modes of the Pacific, namely the PNA and SOI. Multiple linear regression (MLR) is used to derive the linear relationship between the frequency of heavy rain days and the state of ENSO and PNA. Finally, we study the projected future changes in the heavy rain events statistics in relation to projected changes in the joint state of ENSO and PNA modes. For this purpose the emissions scenarios A1B and A2 were analyzed for the mid and late 21st century.

2. Data and Methods

2.1. Daily Rainfall Data

[7] In order to derive the statistical relations between the rainfall event counts and SOI and PNAI, an overlapping observation period is required. From the network of Hawaiian rain gauge stations, we selected 12 stations with daily reported precipitation amounts between 1958–2005 (see Table 1). This period was found to be most suitable for this research based on data availability and homogeneity. The selected stations have the highest ratio of observed to missing reports during the entire time period (80–99% complete). Heavy rainfall events are identified based on the 95% quantiles (p_{95}) in the estimated cumulative frequency distribution of daily precipitation amounts. For each station,

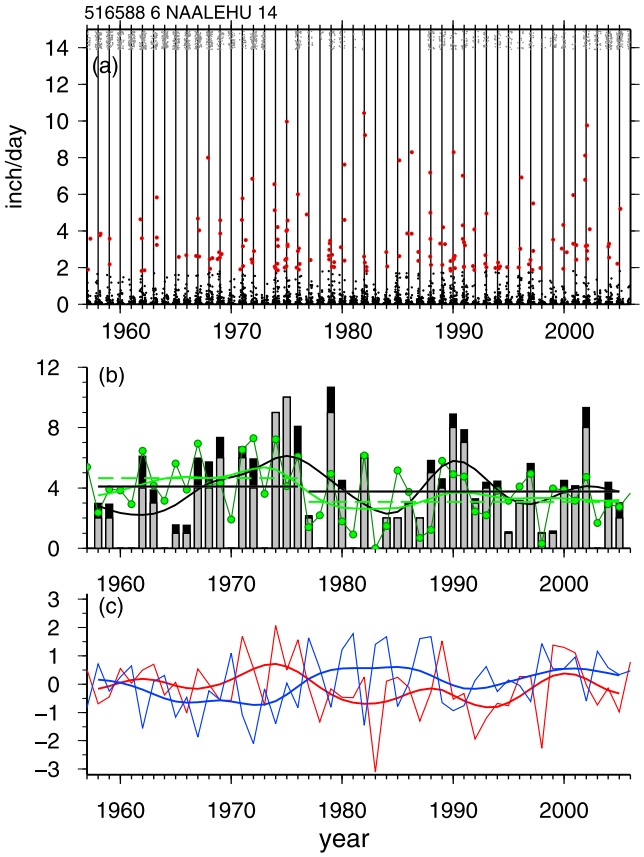

Figure 1. (a) Time series of daily rainfall amounts (black dots; inch/d) at Naalehu (station 11). Heavy rain events are marked in red. Missing days are indicated as gray dots in the upper portion of the graph (above the 14 inch/d level). Note that we randomly shifted the gray dots in the vertical by a small random offset to account for the high data density. (b) Frequency of heavy rain events during the wet season (October-April) 1958–2005. Gray bars are the number of observed events, and black bars denote the corrected number of events accounting for missing observations. Green line with circles is the MLR estimated number of corrected events. The mean of the corrected (black solid line) and MLR estimated (green dashed line) frequency counts is shown for 1958–1976 and 1977–2005 (see also Table 4). (c) Time series of the SOI (red lines) and PNAI (blue lines) seasonally averaged (October-April) based on the data from NOAA's Climate Prediction Center (http://www.cpc.noaa.gov/data/indices/soi; http://www.cpc.ncep.noaa.gov/products/precip/CWlink/pna/pna.shtml). Thick lines in Figures 1b and 1c are the low-pass filtered time series (10 year cutoff period) [*Duchon*, 1979].

p_{95} was determined by sorting all rain days (days with precipitation amounts greater or equal 0.01 inch/d) in a "calibration" period 1958–1976. As will be explained later, this period was selected from the available time range 1958–2005 in order to test if the frequency of events changed after the major climate shift in the mid-1970s [*Trenberth*, 1990; *Diaz et al.*, 2001; *Mantua and Hare*, 2002]. Note that only the wet season (October-April) was considered. The 95% quantile was found to provide a good trade-off between the sample size (i.e., event numbers) and the severity of such events (see Table 1). *Zhang et al.* [2005] found that the estimated exceedance rate can be biased in the case of small sample sizes or high threshold percentiles. They suggested to estimate the exceedance rate within the "in-base period" with Jackknife resampling methods to correct for the bias. In our application we tested to what extend biases could affect the event counts. It was found that the threshold levels for heavy rain events differ only by the order of 0.01 inch/d, which is at the precision limit of the rain gauges. Hence, in this application we do not further apply the bias correction approach.

[8] Since the stations have considerable gaps in the observations during some years, the numbers of events were adjusted in the following way. Assuming the probability of extreme events is independent of the occurrence of missing observations one can correct the number of counted events $\tilde{n}_e(t)$ by:

$$n_e(t) = \tilde{n}_e(t) p_{obs}(t)^{-1}, \quad (1)$$

where $n_e(t)$ is the estimated number of heavy rain events in a wet season year t, $\tilde{n}_e(t)$ is the number of observed events and $p_{obs}(t)$ is the proportion of reported observations during the given wet season. The rationale behind this correction is that the chances of missing an observation is not dependent on the occurrence of heavy rain events. As far as we were able to assess the information on the data recording, archiving and digitization process, this assumption is justified. To illustrate the data processing, Figures 1a and 1b show the daily rainfall amounts and the obtained frequency counts of heavy rain events for one particular station near the southern tip of Big Island. These resulting time series with the number of heavy rain events per wet season (Figure 2) are the target variables in the statistical downscaling (SD) procedure described below.

2.2. Statistical Downscaling Method

[9] In this study, SD is based on multiple linear regression (MLR), in which the number of heavy rain events are assumed to be conditionally dependent on the major modes of climate variability in the North Pacific sector. Initial testing of various combinations of predictors (SOI, Niño 3.4, PDO index, PNA index) indicated that the most robust validation results were obtained with the PNA index and either SOI or Niño 3.4 index. We selected the normalized PNAI and SOI (available at NOAA's Climate Prediction Center (http://www.cpc.noaa.gov/data/indices/soi; http://www.cpc.ncep.noaa.gov/products/precip/CWlink/pna/pna.shtml)) (Figure 1c). The regression patterns [*von Storch and Zwiers*, 1999, p. 380] associated with the SOI and PNAI were obtained from the National Centers for Environmental Prediction- National Center for Atmospheric Research (NCEP- NCAR) reanalysis [*Kalnay et al.*, 1996; *Kistler et al.*, 2001] (seasonally averaged October-April for the years 1961–1990) by using the 1000 hPa and 500 hPa geopotential height fields, respectively. For the SOI regression pattern, we selected the tropical and subtropical region of 30°S–30°N/90°E–280°E. For the PNA pattern the domain extends from the central tropical Pacific to the North American continent (0°S–70°N/120°E–300°E). The regression patterns show the 1000 hPa geopotential height anomalies associated with a

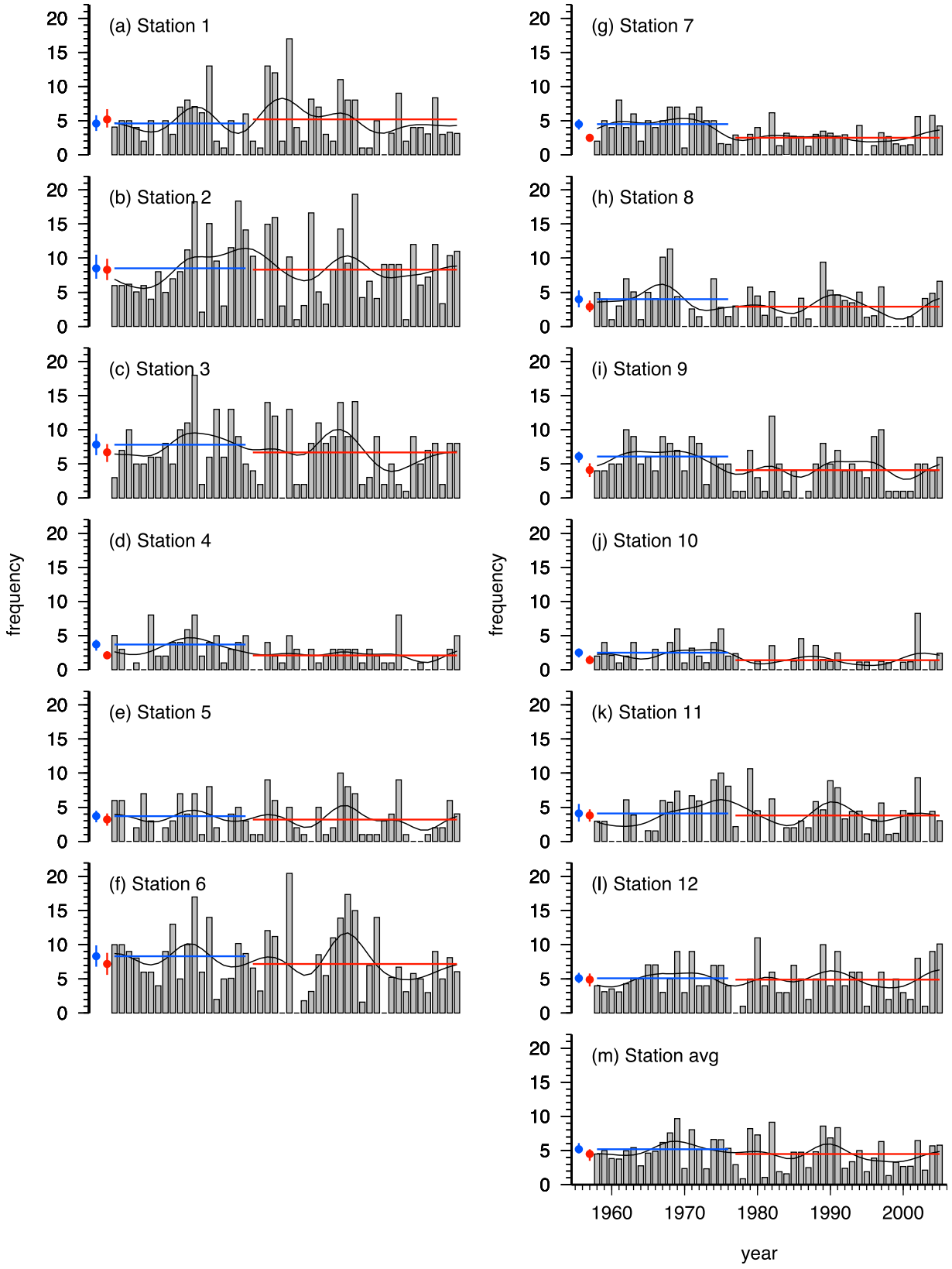

Figure 2. Time series with the number of heavy rain events per wet season during 1958–2005 (a-l) for the 12 stations given in Table 1 and (m) the average of all 12 stations. The 10 year low-pass filtered time series [*Duchon*, 1979] are shown as black lines, and the 1958–1976 (1977–2005) mean number of events are shown as blue (red) lines. Note that the two mean values and their bootstrapped 90% confidence intervals are shown next to the vertical axis for better comparison.

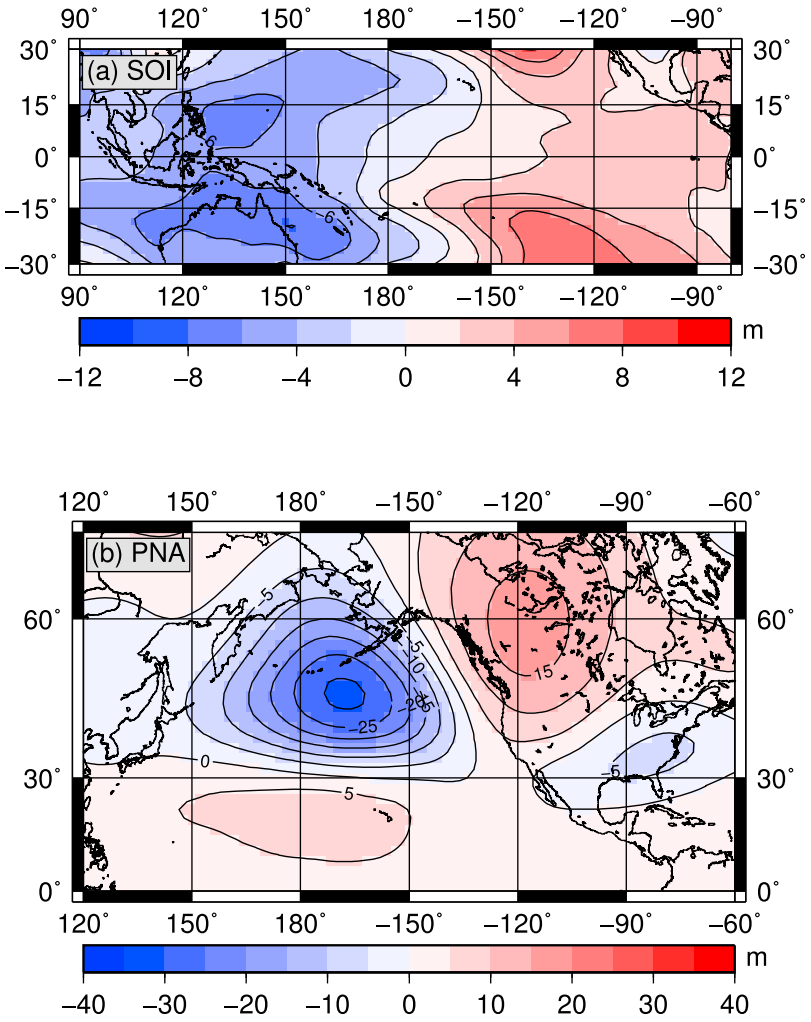

Figure 3. (a) Associated regression pattern of the NCEP reanalysis 1000 hPA geopotential height fields [*Kalnay et al.*, 1996; *Kistler et al.*, 2001] regressed on the SOI calculated using October-April seasonal averages between years 1961 and 1990; (b) same but for the 500 hPa geopotential height fields and the PNAI.

1 standard deviation anomaly in the SOI and the 500 hPa geopotential height anomalies for a 1 standard deviation in the PNAI (Figure 3).

[10] The regression model for a single station can be stated as

$$n_e(t) = a_0 + a_1 SOI(t) + a_2 PNAI(t) + e(t). \qquad (2)$$

[11] In this equation the, number of heavy rain events in a given year t is given by the states of $SOI(t)$ and $PNAI(t)$ and an independent noise component $e(t)$. In the standard maximum likelihood estimation procedure for the MLR it is assumed that predictors and predictands are continuous variables (not discrete count data) and the error terms follow a Gaussian distribution and errors are independent and identically distributed in time. These assumptions are certainly not fulfilled in our case and it should be kept in mind that the regression parameter estimates are not the best linear unbiased estimators. Using resampling techniques for cross validation [*Michaelsen*, 1987], however, we tested the practical performance of the MLR estimates. The regression parameters a_0, a_1, a_2 were calibrated and validated with a Monte Carlo (MC) techniques. The years 1958–2005 were randomly divided (1000 times) into even subsamples (24 years for calibration and validation). Pearson and Spearman correlation coefficients were calculated between the MLR-estimated number of events and the observed number of events for calibration and validation periods during each iteration. Spearman correlation measures the dependency between the estimated and observed number of events by comparing the ranks, where the ranks are determined from the sorted samples (lowest to highest values). This non-parametric measure is more suitable for the event counts than the Pearson correlation. The average values are shown in Table 2, together with the mean regression parameters and their corresponding standard deviations estimated during the cross validation. It must be noted that the estimated significance levels can be affected by serial correlation in the time series of predictors/predictands. We estimated the effects of serial correlation to be small. In no case was the lag-1 autocorrelation significantly different from zero based on a 5% significance test. The estimates for the equivalent

Table 2. Calibration and Validation Statistics of the Monte Carlo MLR Regression for Each Station and the Station Average (AVG)[a]

	Calibration									
	Mean			Standard Deviation			Mean		Validation Mean	
Station	$\hat{a}_0$	$\hat{a}_1$	$\hat{a}_2$	$\hat{a}_0$	$\hat{a}_1$	$\hat{a}_2$	r_p^2	r_s^2	r_p^2	r_s^2
1	5.0	0.62	−1.41	0.53	0.50	0.71	0.24	0.29**	0.18	0.23**
2	8.5	1.67	−1.37	0.64	0.58	0.76	0.30	0.33**	0.25	0.27**
3	7.1	0.79	−1.85	0.56	0.56	0.62	0.33	0.32**	0.27	0.27**
4	2.7	−0.15	−1.01	0.30	0.32	0.30	0.22	0.26**	0.16	0.19**
5	3.4	0.06	−1.41	0.38	0.42	0.45	0.27	0.27**	0.21	0.22**
6	7.7	0.15	−1.74	0.69	0.78	1.00	0.19	0.17*	0.10	0.10
7	3.4	0.10	−1.01	0.29	0.28	0.25	0.28	0.30**	0.24	0.25**
8	3.4	−0.10	−1.39	0.39	0.40	0.42	0.26	0.27*	0.20	0.21**
9	4.9	0.01	−1.98	0.33	0.40	0.36	0.47	0.45**	0.43	0.41**
10	1.9	0.29	−0.39	0.26	0.25	0.29	0.12	0.17*	0.08	0.11
11	3.9	0.63	−1.45	0.38	0.35	0.42	0.37	0.40**	0.33	0.36**
12	5.0	0.23	−0.83	0.38	0.39	0.46	0.17	0.22*	0.11	0.15
AVG	4.7	0.36	−1.32	0.27	0.27	0.34	0.45	0.48**	0.40	0.44**

[a]The mean of the estimated regression coefficients in equation (2) and their standard deviation are given ($\hat{a}_{0,1,2}$). Mean values of the squared Pearson and Spearman correlations (r_p^2 and r_s^2, respectively) are shown for the calibration and validation; 10% (5%) one-sided significance (null hypothesis: zero correlation) levels are indicated by *(**) for the Spearman correlations only. Tests were calculated using the statistical software package R (K. Hornik, The R FAQ, 2010, http://www.ci.tuwien.ac.at/hornik/R/R-FAQ.html).

sample size [*von Storch and Zwiers*, 1999, p. 115] deviate less than 10% from the nominal sample size.

[12] Data for the AR4 twentieth century climate model simulations and the twenty-first-century simulations for CO_2 emissions scenarios A1B and A2 were obtained from the FTP server (ftp-esg.ucllnl.org) maintained by the Earth System Grid II (ESG) research project sponsored by the U.S. Department of Energy Office of Science. We selected six models for the current analysis (see Table 3) that represent a wide range of projected mean precipitation changes for Hawaii [*Timm and Diaz*, 2009]. Geopotential height data from the models were interpolated onto the NCEP grid (2.5° × 2.5°) using bicubic interpolation. SOI and PNAI were obtained by projecting the 1000 hPa and 500 hPa geopotential height fields onto their associated regression patterns from the NCEP reanalysis. The time-dependent geopotential height fields were projected onto the regression patterns for the years 1961–1990, 2046–2065 and 2081–2100. The period 1961–1990 of the "20c3m" scenario simulations were used to define present-day reference climate statistics. For each model, we normalized the projection indices to have zero mean and unit variance for the the 20th century period. The same offset and scaling factors are subsequently applied to the future climate change scenarios in 2046–2065 and 2081–2100. Note that the general warming trend in the 21st century leads to an overall increase in the height of 500 hPa geopotential and we removed this signal from the projected PNAI.

3. Results

[13] In this section we present the calibration and cross validation of the multiple linear regression (MLR) model which forms the core of the SD process, and the analysis of the six-member model ensemble with respect to their future

Table 3. Simulated Changes in the Mean and Variance of SOI and PNAI in Six Models of the IPCC AR4 Report[a]

	SOI 2046–2065 (2081–2100)		PNAI 2046–2065 (2081–2100)	
Model	Mean	Variance	Mean	Variance
	Emissions Scenario A1B			
CCCMA_CGCM3_1	0.33 (0.61*)	1.70 (0.47)	0.94* (0.52*)	1.13 (1.12)
GFDL_CM2_0	0.16 (−0.06)	0.64 (0.85)	−0.55 (0.19)	1.70 (1.27)
GFDL_CM2_1	0.24 (0.30)	0.14* (0.17*)	0.31 (0.16)	0.62 (1.03)
MPI_ECHAM5	−0.22 (−0.44)	1.80 (1.59)	−0.15 (0.45)	1.30 (1.08)
MRI_CGCM2_3_2a[a]	−0.62* (−0.45)	1.26 (1.11)	0.42 (0.47)	1.75 (1.84*)
UKMO_HADCM3	0.05 (−0.17)	1.27 (0.99)	−0.07 (−0.51*)	3.41* (1.32)
Ensemble mean	−0.01 (−0.04)	1.19 (0.98)	0.15 (0.21*)	1.79 (1.34)
	Emissions Scenario A2			
CCCMA_CGCM3_1	0.27 (1.07*)	0.91 (1.23)	0.66* (0.83*)	0.78 (0.48)
GFDL_CM2_0	−0.01(0.12)	0.80 (0.97)	0.12 (0.02)	0.98 (1.14)
GFDL_CM2_1	0.10 (0.36)	0.67 (0.38)	0.11 (−0.20)	0.89 (1.19)
MPI_ECHAM5	−0.45 (−0.20)	1.58 (1.32)	0.09 (0.38)	1.65 (1.65)
MRI_CGCM2_3_2a[a]	−0.51 (−0.69*)	1.90 (1.98)	0.49* (0.83*)	1.21 (0.69)
UKMO_HADCM3	−0.03 (−0.09)	1.62 (1.54)	−0.51 (−0.78*)	1.69 (3.24)
Ensemble mean	−0.01 (−0.01)	1.27 (1.48)	0.16 (0.18)	1.28 (1.68)

[a]The years 1961–1990 from the 20th century run 20C3M were used as a reference period: the mean of the SOI and PNAI during the 1961–1990 period was subtracted, and the anomalies were scaled by the standard deviation 1961–1990. Differences passing the two-sided 5% Bootstrap significance test (null hypothesis: difference is zero) are marked with an asterisk.

Table 4. Average Wet-Season Frequency of Heavy Rain Events During the Period 1958–1976 and 1977–2005[a]

	Observed		MLR Estimates	
Station	1958–1976	1977–2005	1958–1976	1977–2005
1	4.6	5.2	5.9	4.4*
2	8.6	8.3	9.7	7.6*
3	7.8	6.7	8.3	6.4*
4	3.7	2.1*	3.1	2.4*
5	3.7	3.2	4.1	2.9*
6	8.3	7.2*	8.7	7.1*
7	4.5	2.5*	3.9	3.0*
8	4.0	2.9	4.0	2.9*
9	6.1	4.1*	5.9	4.3*
10	2.5	1.4*	2.1	1.6*
11	4.1	3.8	4.8	3.3*
12	5.1	4.9	5.5	4.7*
Average	5.2	4.5	5.5	4.2*

[a]Observations are taking the correction for missing observations into account. Significant differences between the two periods were tested with Monte Carlo techniques. Note that the MLR estimates are all significant due to the simultaneous changes in SOI and PNAI. One-sided 5% significance for downward trends is marked with an asterisk.

projection of changes in SOI and PNAI. The target variables (predictands) are the time series of the frequency of heavy rain events per wet season (October-April) shown in Figure 2. The time series show variability on interannual, decadal and multidecadal time scales. The long-term average of heavy rain events per season is highly variable among the stations as a result of different number of dry days. For example, Hilo (station 2) has on average 8–9 heavy rain events per season (212 days (213 for leap years)) whereas the high-elevation station on Mauna Loa (10) has only 1–3 events in one season.

3.1. MLR Model Cross Validation and Application to the Mid-1970s Climate Shift

[14] We applied a MC cross-validation technique by randomly drawing 24 years (without repetition) from 1958–2005 for the calibration of the MLR model and using the remaining years for validation of the model. The results are summarized in Table 2. Three stations did not pass the null hypothesis test for zero correlation at the 10% significance level for the Spearman rank correlation. For those stations, cross-validation analysis resulted in the null hypothesis being rejected for more than 70% of the 1000 subsamples. In case of stations "Kailua 446" and "Mauna Loa Slope Obs" average p values were larger than 10% (station "Opihipihi Hale 2 24" larger than 9%). For the significant stations the average ranked Spearman correlations are between 0.42 and 0.66 in the validation samples. Accordingly, about 18–44% of the interannual to decadal variability in the number of heavy rain events can be explained by SOI and PNAI variability.

[15] For the application to future climate change, it is important that the statistical relationships can be applied to changes in the long-term mean. Here we test to what extent the calibrated MLR model is capable of reproducing the observed climate shift in the mid-1970s that affected the climate of the North Pacific [*Trenberth*, 1990; *Graham*, 1994; *Mantua et al.*, 1997; *Mantua and Hare*, 2002; *Meehl et al.*, 2009]. We calculated the average frequency of heavy rain events (wet season) for the years 1958–1976 and 1977–2005. Nine of the 12 stations indicate a negative trend, five of them are significant (5% one-sided test for null hypothesis of equal means, see Table 4). Only one station indicated an increase in heavy rain events (not significant). The significance of the differences in the mean frequency was tested with Bootstrap sampling techniques [*Efron and Tibshirani*, 1993]. From the pooled sample (i.e., all years 1958–2005 combined), we randomly selected (with replacement) 19 and 29 year subsamples, calculated the differences and estimated confidence ranges.

[16] The MLR model in our application uses the information from SOI and PNAI and accordingly a reduction in the heavy rain events can be produced in various combinations of SOI-PNAI shifts. Between the periods 1958–1976 and 1977–2005 the SOI and PNAI experienced a mean shift from a weakly positive to negative mean state in the SOI, and from negative to positive PNAI (Figure 4). Despite the large year-to-year variability, the mean changes appear significant (two-sided 10% significance test based on Bootstrap confidence estimates for the differences in the mean). The variance of SOI has slightly increased in the latter period, although this change is not significant according to the MC test. The variance of the PNA and its covariance with the SOI appear unaffected by the climate shift (statistically not significantly different between the two periods according to two-sided 10% significance test with Bootstrap method).

[17] Applying the MLR model with the SOI and PNAI changes, the shift in the number of heavy rain events after

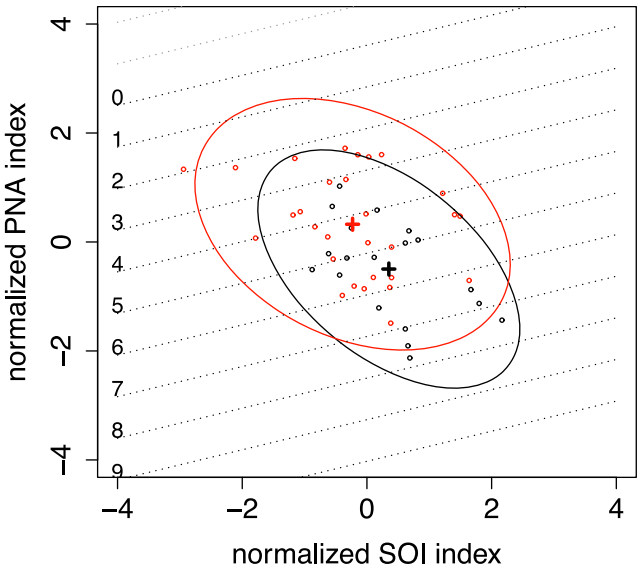

Figure 4. Phase-space presentation of the tropical and North Pacific atmospheric circulation in the SOI and PNAI subspace for the periods 1958–1976 and 1977–2005. Each year is marked by small circles in black and red for the former and latter period, respectively. Mean states are shown as crosses for the two subperiods. Ellipses mark the approximate 95% range for a two-dimensional Gaussian distribution with mean and covariance estimates from the samples (same color code applies). Dotted lines illustrate the MLR estimates of the number of heavy rain events for the average of all 12 stations.

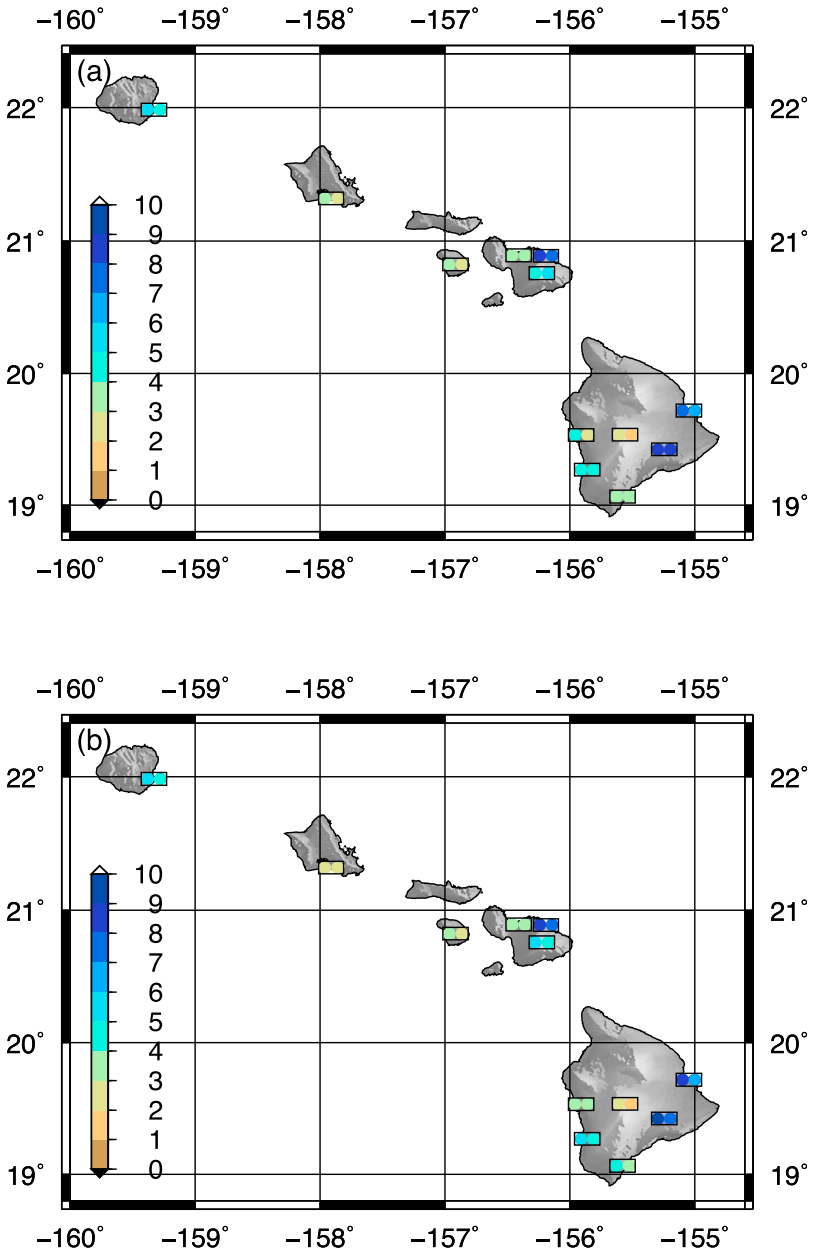

Figure 5. Map showing the local changes observed during the mid-1970s climate shift: (a) average number of heavy rain events in the observations corrected for missing data (see Table 4). For each station, the mean of the 1958–1976 (1977–2005) period is indicated by the colors on left (right) side. (b) Same as Figure 5a but the estimated means use the MLR model.

1976 can be reproduced (see Table 4). Since the SOI and PNAI changes both result in a reduction of heavy rain events, the MLR model gives statistically significant decreasing number of events. Figure 5 highlights that the negative trend is widespread across the islands. It is important to recall that the mean changes in the observations were calculated after correcting for missing observations. The low biases between SD estimates and the observed mean values demonstrate that the correction method works even if the number of missing observations differs considerably in the two time intervals (see Tables 1 and 4, stations 6, 7, 8, 10, and 11). In summary, the capabilities of the MLR model in reproducing changes on interdecadal time scales lends further credence to its application for future climate change projections [e.g., *Charles et al.*, 2004]. Further support will have to come from dynamical downscaling models [*Vrac et al.*, 2007].

3.2. Future Changes in the SOI, PNA, and Number of Heavy Rain Events

[18] We have analyzed six models from the AR4 database and projected the simulated geopotential height fields onto the SOI and PNA regression pattern shown in

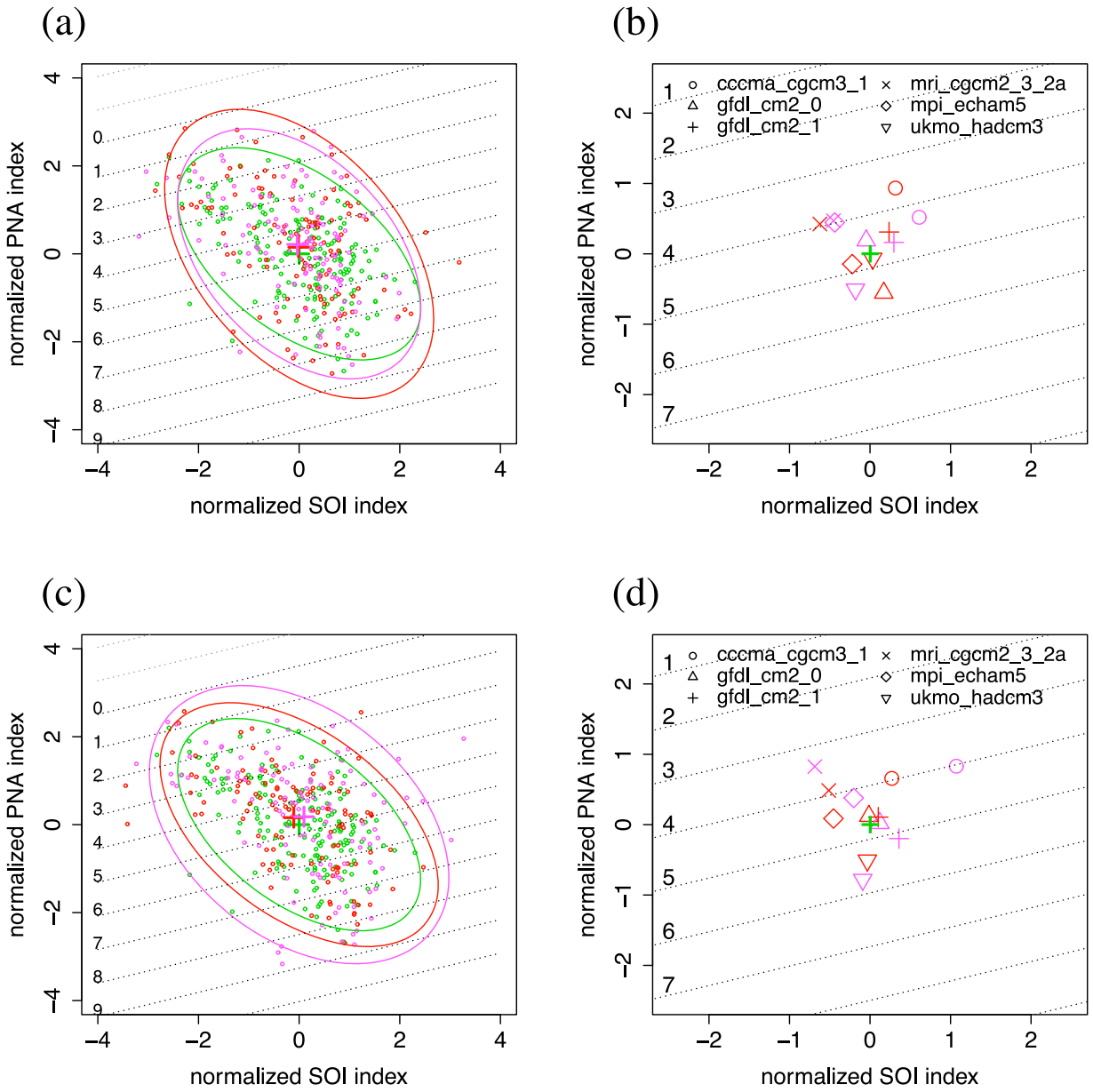

Figure 6. Modeled SOI and PNAI for the present-day climate (1961–1990, green), and future climate change scenarios in the mid (2046–2065, red) and late (2081–2100, purple) 21st century. (a) Phase-space representation of the six-model ensemble for emissions scenario A1B. Ellipses mark the approximate 95% range for a two-dimensional Gaussian distribution with mean and covariance estimates from the samples (same color code applies). Dotted lines illustrate the MLR estimates of the number of heavy rain events for the average of all 12 stations. (c) Same as Figure 6a but for the ensemble for emissions scenario A2. (b) The simulated changes in the mean relative to present (green cross) are shown for the individual models (red, mean of 2046–2065; purple, mean of 2081–2100) for emissions scenario A1B. (d) Same as Figure 6b but for emissions scenario A2.

Figure 3. Two different emissions scenarios and two different time intervals of the 21st century were studied. In general we find that the simulated changes in the SOI and PNAI mean states, their variability, and covariance are small. Below we concentrate on the most robust changes that are statistically significant, and models that show the same sign in the anomalies in both scenarios and both time segments.

3.2.1. Changes in the Mean

[19] The mean changes relative to the models' present-day climate simulations indicate relatively small changes in the A1B and A2 scenario runs in the mid and late 21st century (Table 3). The CCCMA model simulates positive anomalies in the SOI in both scenarios that become significantly different from the null hypothesis of no mean change (5% significance level). The same tendency is found in the

Table 5. Simulated Changes in the Covariance Between SOI and PNAI in Six Models of the IPCC AR4 Report[a]

Model/Observations	20th Century 1961–1990 (1950–2009)	Scenario A1B 2046–2065 (2081–2100)	Scenario A2 2046–2065 (2081–2100)
NCEP reanalysis	(−0.47)	-	-
CCCMA_CGCM3_1	−0.30	−0.67 (−0.26)	−0.08 (−0.07)
GFDL_CM2_0	−0.62	−0.47 (−0.47)	−0.34 (−0.65)
GFDL_CM2_1	−0.73	−0.18 (−0.16)	−0.46 (−0.42)
MPI_ECHAM5	−0.38	−0.67 (−0.72)	−0.89 (−0.88)
MRI_CGCM2_32[a]	−0.76	−0.75 (−0.92)	−0.76 (−0.30)
UKMO_HADCM3	−0.31	−1.50 (−0.67)	−1.21* (−1.35*)
Ensemble mean	−0.51	−0.65 (−0.48)	−0.63 (−0.59)

[a]Covariance changes between the 20th and 21st century were tested with bootstrap resampling using a two-sided 5% significance test (significant changes are marked with asterisks).

GFDL_CM2_1 model; however, it is nonsignificant. Two models indicate negative anomalies in theSOI mean state, but only in case of the MRI model is statistical significance reached. The remaining models do not indicate robust changes in the SOI. Moreover, the ensemble mean does not indicate any significant change.

[20] The PNA analysis shows that the CCCMA model has a significant shift toward a more positive mean PNA state as is the case for the MRI model (significant only for the A2 scenario, though). The UKMO model on the other hand indicates a tendency toward a more negative PNA mean state. Given the known negative correlation on interannual and decadal time scales between SOI and PNA in the past, it is interesting to note that the CCCMA model seems to produce in-phase mean anomalies in the future scenarios, whereas the out-of-phase relationship is observed in the MRI model. As for the SOI, mean changes in PNAI are small in the ensemble mean and marginally significant. The magnitude of the modeled future mean shifts in the SOI-PNAI phase state are small compared to the mid-1970s shift. The mean changes during the mid-1970s climate shift are about 0.6 for the SOI and 0.8 for the PNAI, and the modeled mid to late 21st century changes are in the same range as the differences between the pre- and post-1970s climate shift (see Figure 6 and Table 3).

3.2.2. Changes in the Variance and Covariance

[21] Due to the covariance between PNA and ENSO, it is clear that future climate change and its consequences for the frequency of heavy rain events in Hawaii are affected more than just by changes in the mean climate states. Increases in the interannual variability or in the covariance between ENSO and PNA could change the variability in the number of heavy rain events. The models reproduce the observed 20th century correlation between the normalized indices quite well. Note that the variance of the modeled SOI and PNAI were rescaled to have unit variance in the 20th century interval 1961–1990 and the same scaling factor was applied to the scenario simulations. The SOI variability does not change significantly in the model ensemble of the A1B scenario. A more systematic increase in SOI variability is simulated in the A2 scenario, but statistical significance was not detected (Table 3).

[22] No robust systematic changes in the PNA variability are detected when comparing the individual models between their A1B and A2 scenario simulations. However, the ensemble mean seems to indicate a weak increase (statistically not significant according to the two-sided 5% Bootstrap significance test). This behavior appears to be biased by the UKMO model, which produces intermittently a threefold increase in the PNA variability (Table 3).

[23] Whereas individual model scenarios show some distinctive changes in the covariance structures (e.g., UKMO_HADCM3 during the end of the 21st century), no consistent changes can be deduced from the model ensemble (Table 5). We applied the Bootstrap test on the null hypothesis that the covariance of the pre and post climate shift period are equal. The differences between the covariances did not pass the two-sided 5% significance test, except for the UKMO_HADCM3 model. The constancy of the covariance throughout the 21st century scenario simulations is suggestive of a stable teleconnection process between the tropical and extratropical Pacific climate mode in a globally warming climate.

4. Discussion

[24] As was shown in the cross validation, only 18–44% of the interannual to decadal variability in the number of wet season heavy rain days is explained by the SD model. The remaining part of the variability, which is either controlled by other climate modes or local-scale processes, must be studied with complementary statistical or dynamical modeling methods. The lack of significant changes in ENSO or PNA does not exclude the possibility of significant future changes in the heavy rain event statistics. The general increase of precipitable water in a warming atmosphere according to the Clausius-Clapeyron equation will increase the overall potential for heavy rain events. However, locally operating feedbacks between increased ocean SST and convection for example [*Xie et al.*, 2010], or changes in the Hadley Circulation [*Vecchi et al.*, 2006; *Held and Soden*, 2006] can impose strong dynamical control on the regional distribution of the water vapor in the atmosphere. To assess the risk of more intense heavy rainfall events due to enhanced precipitable water in the atmosphere, one must deploy regional modeling studies, in which the interaction between thermodynamic and dynamical processes can be studied explicitly.

[25] With expected improvements in the modeling capabilities in the next generation IPCC scenario runs, it is possible that more robust estimates for the state of Pacific climate modes will be achieved. The future changes reported in Tables 3 and 5 fail to present consistent signs in the projected mean changes. Moreover, the variance and

covariance indicate no systematic increase in the amplitudes of the projected changes toward the end of the 21st century. This could be caused by the rather large internal multi-decadal variability that confounds our efforts to detect the CO_2-forced signals. Twenty year sampling periods may, therefore, be insufficient for the detection of weak signals. Improvements in the detection of future changes could be achieved by including an extended multimodel ensemble analysis, which would increase the signal-to-noise ratio in the detection of mean or covariance changes between tropical ENSO variability and the extratropical PNA climate mode. However, the recent study of *Oshima and Tanimoto* [2010] and *Oshima et al.* [2010, and personal communication, 2010] showed that ensemble averages can only reduce a fraction of the uncertainty surrounding the future anomaly estimates.

[26] Overall, a trend toward fewer heavy rain events has been observed in Hawaii between the periods 1958–1976 and 1977–2005. This observation is in agreement with the recent statistical analyses of *Levinson and Kruk* [2008] and *Chu et al.* [2010], who also found a decreasing trend in the number of extreme events and the rainfall amounts during extreme events. Earlier results have reported that the number of extreme rain events in Hawaii has increased during the last 50 years [*Kunkel et al.*, 2008, and references therein]. However, it is difficult to assess whether this apparent conflict is due to the use of different definitions of extreme events or to the different processing of the station rain gauge data [*Kunkel et al.*, 2003; *Groisman et al.*, 2004, 2005]. The methodology of *Groisman et al.* [2005], for example, was developed for continental extratropical stations. The results from the MLR demonstrated that the combined effects of tropical ENSO-related climate variability and the winter circulation over the extratropical North Pacific are equally important for the interannual to decadal variability in the frequency of heavy rain events. Connections to the PDO, which plays a dominant role in the low-frequency variability of the North Pacific Ocean and the overlying atmosphere [*Yu and Zwiers*, 2007] are difficult to integrate into the MLR models used for the statistical downscaling. The PDO index has a strong autocorrelation, which reduces the equivalent sample size [*von Storch and Zwiers*, 1999, p. 115], and with the limited record lengths for daily rainfall data, the regression parameter would have a large uncertainty. Earlier studies used the PDO index rather than the PNA for their rainfall analysis [*Chu*, 1995; *Chu et al.*, 2010]. However, the amount of independent information about the rainfall in Hawaii, which could be extracted from the PDO-related SST variability, is small because of the close relationship between PDO, PNA and ENSO variability [*Schneider and Cornuelle*, 2005; *Yu and Zwiers*, 2007].

[27] The extent to which the differences before and after the mid-1970s climate shift are attributable to natural or anthropogenic forcing cannot be answered with high confidence [*Meehl et al.*, 2009] due to the lack of long-term climate and rainfall information from the past decades and centuries, and due to insufficient understanding of how external forcing and internal processes control ENSO, PNA, and PDO. Since the ratio between natural and forced variability in current AOGCMs is still uncertain, single model experiments must be considered with some caution regarding their universality. In the presence of these remaining uncertainties, our ability to project changes in the number of heavy rain events is limited.

[28] **Acknowledgments.** O. Elison Timm is supported by the Japan Agency for Marine-Earth Science and Technology (JAMSTEC) through its sponsorship of the International Pacific Research Center. H. F. Diaz received support from the NOAA Office of Climate Programs, the USGS Pacific Island Ecosystems Research Center (PIERC), and the U.S. Department of Energy, Office of Energy Research. T. W. Giambelluca and M. Takahashi were supported by the National Oceanic and Atmospheric Administration (award NA09OAR4310103), the USGS PIERC, and the U.S. Fish and Wildlife Service through the Pacific Island Climate Change Cooperative. We thank the anonymous reviewers for their constructive comments. This is International Pacific Research Center contribution 744 and School of Ocean and Earth Science and Technology contribution 8065.

References

Cao, G., T. W. Giambelluca, D. E. Stevens, and T. A. Schroeder (2007), Inversion variability in the Hawaiian trade wind regime, *J. Clim.*, *20*(7), 1145–1160, doi:10.1175/JCLI4033.1.

Charles, S. P., B. C. Bates, I. N. Smith, and J. P. Hughes (2004), Statistical downscaling of daily precipitation from observed and modelled atmospheric fields., *Hydrol. Processes*, *18*, 1373–1394, doi:10.1002/hyp.1418.

Christensen, J., et al. (2007), Regional climate projections, in *Climate Change 2007—The Physical Science Basis. Contribution of Working Group I to the Fourth Assessment Report of the IPCC*, chap. 11, pp. 849–926, Cambridge Univ. Press, Cambridge, U. K.

Chu, P.-S. (1989), Hawaiian droughts and the Southern Oscillation, *Int. J. Climatol.*, *9*, 619–631.

Chu, P.-S. (1995), Hawaii rainfall anomalies and El Niño, *J. Clim.*, *8*(6), 1697–1703, doi:10.1175/1520-0442(1995)008<1697:HRAAEN>2.0.CO;2.

Chu, P.-S., and H. Chen (2005), Interannual and interdecadal rainfall variations in the Hawaiian Islands, *J. Clim.*, *18*(22), 4796–4813, doi:10.1175/JCLI3578.1.

Chu, P.-S., X. Zhao, Y. Ruan, and M. Grubbs (2009), Extreme rainfall events in the Hawaiian Islands, *J. Appl. Meteorol. Climatol.*, *48*(3), 502–516, doi:10.1175/2008JAMC1829.1.

Chu, P.-S., Y. R. Chen, and T. A. Schroeder (2010), Changes in precipitation extremes in the Hawaiian Islands in a warming climate, *J. Clim.*, *23*(18), 4881–4900. doi:10.1175/2010JCLI3484.1.

Collins, M. (2005), El Niño- or la Niña-like climate change?, *Clim. Dyn.*, *24*, 89–104, doi:10.1007/s00382-004-0478-x.

Collins, M., et al. (2010), The impact of global warming on the tropical Pacific Ocean and El Niño, *Nat. Geosci.*, *3*(6), 391–397, doi:10.1038/NGEO868.

Diaz, H. F., M. P. Hoerling, and J. K. Eischeid (2001), ENSO variability, teleconnections and climate change, *Int. J. Climatol.*, *21*, 1845–1862, doi:10.1002/joc.631.

Diaz, H. F., P. S. Chu, and J. K. Eischeid (2005), Rainfall changes in Hawaii during the last century, paper presented at 16th Conference on Climate Variability and Change, Am. Meteorol. Soc., San Diego, Calif. (Available at http://ams.confex.com/ams/Annual2005/techprogram/paper_84210.htm)

Duchon, C. E. (1979), Lanczos filtering in one and two dimensions, *J. Appl. Meteorol.*, *18*(8), 1016–1022, doi:10.1175/1520-0450(1979)018<1016:LFIOAT>2.0.CO;2.

Efron, B., and R. J. Tibshirani (1993), *An Introduction to the Bootstrap*, *Monogr. Stat. Appl. Prob.*, vol. 57, 436 pp., Chapman and Hall, New York.

Giambelluca, T. W., H. F. Diaz, and M. S. A. Luke (2008), Secular temperature changes in Hawai'i, *Geophys. Res. Lett.*, *35*, L12702, doi:10.1029/2008GL034377.

Graham, N. E. (1994), Decadal-scale climate variability in the tropical and North Pacific during the 1970s and 1980s: Observations and model results, *Clim. Dyn.*, *10*, 135–162, doi:10.1007/BF00210626.

Groisman, P. Y., R. W. Knight, T. R. Karl, D. R. Easterling, B. Sun, and J. H. Lawrimore (2004), Contemporary changes of the hydrological cycle over the contiguous United States: Trends derived from in situ observations, *J. Hydrometeorol.*, *5*(1), 64–85, doi:10.1175/1525-7541(2004)005<0064:CCOTHC>2.0.CO;2.

Groisman, P. Y., R. W. Knight, D. R. Easterling, T. R. Karl, G. C. Hegerl, and V. N. Razuvaev (2005), Trends in intense precipitation in the climate record, *J. Clim.*, *18*(9), 1326–1350, doi:10.1175/JCLI3339.1.

Hegerl, G. C., F. W. Zwiers, P. A. Stott, and V. V. Kharin (2004), Detectability of anthropogenic changes in annual temperature and precipitation extremes, *J. Clim.*, *17*(19), 3683–3700, doi:10.1175/1520-0442(2004)017<3683:DOACIA>2.0.CO;2.

Held, I. M., and B. J. Soden (2006), Robust responses of the hydrological cycle to global warming, *J. Clim.*, *19*(21), 5686–5699, doi:10.1175/JCLI3990.1.

Kalnay, E., et al. (1996), The NCEP/NCAR 40-year reanalysis project, *Bull. Am. Meteorol. Soc.*, *77*, 437–471.

Kistler, R., et al. (2001), The NCEP-NCAR 50-year reanalysis: Monthly means CD-ROM and documentation, *Bull. Am. Meteorol. Soc.*, *82*, 247–267, doi:10.1175/1520-0477(2001)082<0247:TNNYRM>2.3.CO;2.

Kunkel, K. E., D. R. Easterling, K. Redmond, and K. Hubbard (2003), Temporal variations of extreme precipitation events in the United States: 1895–2000, *Geophys. Res. Lett.*, *30*(17), 1900, doi:10.1029/2003GL018052.

Kunkel, K. E., et al. (2008), Observed changes in weather and climate extremes, in *Weather and Climate Extremes in a Changing Climate: Regions of Focus: North America, Hawaii, Caribbean, and U.S. Pacific Islands*, edited by T. R. Karl et al., pp. 35–80, U.S. Clim. Change Sci. Program, Washington, D. C.

Latif, M., and N. S. Keenlyside (2009), El Niño/Southern Oscillation response to global warming, *Proc. Natl. Acad. Sci. U. S. A.*, *106*(49), 20,578–20,583, doi:10.1073/pnas.0710860105.

Levinson, D. H., and M. C. Kruk (2008), Evaluating the impacts of climate change on rainfall extremes for Hawaii and coastal Alaska, paper presented at 24th Conference on Severe Local Storms, Am. Meteorol. Soc., Savannah, Ga. (Available at http://ams.confex.com/ams/24SLS/techprogram/paper_142172.htm)

Lyons, S. W. (1982), Empirical orthogonal function analysis of Hawaiian rainfall, *J. Appl. Meteorol.*, *21*(11), 1713–1729, doi:10.1175/1520-0450(1982)021<1713:EOFAOH>2.0.CO;2.

Mantua, N. J., and S. R. Hare (2002), The Pacific Decadal Oscillation, *J. Oceanogr.*, *58*(1), 35–44, doi:10.1023/A:1015820616384.

Mantua, N. J., S. R. Hare, Y. Zhang, J. M. Wallace, and R. C. Francis (1997), A Pacific interdecadal climate oscillation with impacts on salmon production, *Bull. Am. Meteorol. Soc.*, *78*, 1069–1079, doi:10.1175/1520-0477(1997)078<1069:APICOW>2.0.CO;2.

Meehl, G. A., A. Hu, and B. D. Santer (2009), The mid-1970s climate shift in the Pacific and the relative roles of forced versus inherent decadal variability, *J. Clim.*, *22*(3), 780–792, doi:10.1175/2008JCLI2552.1.

Michaelsen, J. (1987), Cross-validation in statistical climate forecast models, *J. Clim. Appl. Meteorol.*, *26*(11), 1589–1600, doi:10.1175/1520-0450(1987)026<1589:CVISCF>2.0.CO;2.

Oki, D. S. (2004), Trends in streamflow characteristics at long-term gaging stations, Hawaii, *Sci. Invest. Rep. 2004-5080*, U.S. Geol. Surv., Denver, Colo.

Oshima, K., and Y. Tanimoto (2010), An evaluation of reproducibility of the Pacific Decadal Oscillation in the CMIP3 simulations, *J. Meteorol. Soc. Jpn.*, *84*(4), 755–770, doi:10.2151/jmsj.87.755.

Oshima, K., Y. Tanimoto, and S.-P. Xie (2010), Regional patterns of SST warming trend in the North Pacific based on CMIP3 mulit-model simulations, Abstract GC13C-0706 presented at Fall Meeting, AGU, San Francisco, Calif., 13–17 Dec.

Schneider, N., and B. D. Cornuelle (2005), The forcing of the Pacific Decadal Oscillation, *J. Clim.*, *18*(21), 4355–4373, doi:10.1175/JCLI3527.1.

Schroeder, T. A. (1993), Climate controls, in *Prevailing Trade Winds: Weather and Climate in Hawai'i*, edited by M. Sanderson, p. 12–36, Univ. of Hawai'i Press, Honolulu.

Stott, P. A., N. P. Gillett, G. C. Hegerl, D. J. Karoly, D. A. Stone, X. Zhang, and F. Zwiers (2010), Detection and attribution of climate change: A regional perspective, *Wiley Interdisciplinary Rev. Clim. Change*, *1*, 192–211, doi:10.1002/wcc.34.

Timm, O., and H. F. Diaz (2009), Synoptic-statistical approach to regional downscaling of IPCC 21st century climate projections: Seasonal rainfall over the Hawaiian Islands, *J. Clim.*, *22*(16), 4261–4280, doi:10.1175/2009JCLI2833.1.

Trenberth, K. (1990), Recent observed interdecadal climate changes in the Northern Hemisphere, *Bull. Am. Meteorol. Soc.*, *71*, 988–993, doi:10.1175/1520-0477(1990)071<0988:ROICCI>2.0.CO;2.

Vecchi, G. A., and A. T. Wittenberg (2010), El Niño and our future climate: Where do we stand?, *Wiley Interdisciplinary Rev. Climate Change*, *1*(2), 260–270, doi:10.1002/wcc.33.

Vecchi, G. A., B. J. Soden, A. T. Wittenberg, I. M. Held, A. Leetmaa, and M. J. Harrison (2006), Weakening of tropical Pacific atmospheric circulation due to anthropogenic forcing, *Nature*, *441*, 73–76, doi:10.1038/nature04744.

von Storch, H., and F. Zwiers (1999), *Statistical Analysis in Climate Research*, 484 pp., Cambridge Univ. Press, Cambridge, U. K.

Vrac, M., M. L. Stein, K. Hayhoe, and X. Liang (2007), A general method for validating statistical downscaling methods under future climate change, *Geophys. Res. Lett.*, *34*, L18701, doi:10.1029/2007GL030295.

Wilby, R., and T. Wigley (1997), Downscaling general circulation model output: A review of methods and limitations, *Prog. Phys. Geogr.*, *21*, 530–548, doi:10.1177/030913339702100403.

Xie, S.-P., C. Deser, G. A. Vecchi, J. Ma, H. Teng, and A. T. Wittenberg (2010), Global warming pattern formation: Sea surface temperature and rainfall, *J. Clim.*, *23*(4), 966–986, doi:10.1175/2009JCLI3329.1.

Yu, B., and F. Zwiers (2007), The impact of combined ENSO and PDO on the PNA climate: A 1,000-year climate modeling study, *Clim. Dyn.*, *29*, 837–851, doi:10.1007/s00382-007-0267-4.

Zhang, X., G. Hegerl, F. W. Zwiers, and J. Kenyon (2005), Avoiding inhomogeneity in percentile-based indices of temperature extremes, *J. Clim.*, *18*(11), 1641–1651, doi:10.1175/JCLI3366.1.

Zhang, X., F. W. Zwiers, G. C. Hegerl, F. H. Lambert, N. P. Gillett, S. Solomon, P. A. Stott, and T. Nozawa (2007), Detection of human influence on twentieth-century precipitation trends, *Nature*, *448*, 461–464, doi:10.1038/nature06025.

Zwiers, F. W., and X. Zhang (2003), Toward regional-scale climate change detection, *J. Clim.*, *16*(5), 793–797, doi:10.1175/1520-0442(2003)016<0793:TRSCCD>2.0.CO;2.

O. Elison Timm, International Pacific Research Center, SOEST, University of Hawai'i at Mānoa, 1680 East-West Rd., POST Bldg. 401, Honolulu, HI 96822, USA. (timm@hawaii.edu)

T. W. Giambelluca and M. Takahashi, Department of Geography, University of Hawai'i at Mānoa, 2424 Maile Way, Honolulu, HI 96822, USA.

H. F. Diaz, Climate Diagnostics Center, NOAA-CIRES, 325 Broadway, Boulder, CO 80305, USA.